Supplemental Information

Proteomics links ubiquitin chain topology change to transcription factor activation

Yanchang Li, Eric B. Dammer, Yuan Gao, Qiuyan Lan, Mark A. Villamil, Duc M. Duong, Chengpu Zhang, Lingyan Ping, Linda Lauinger, Karin Flick, Zhongwei Xu, Wei Wei, Xiaohua Xing, Lei Chang, Jianping Jin, Xuechuan Hong, Yunping Zhu, Junzhu Wu, Zixin Deng, Fuchu He, Peter Kaiser, and Ping Xu

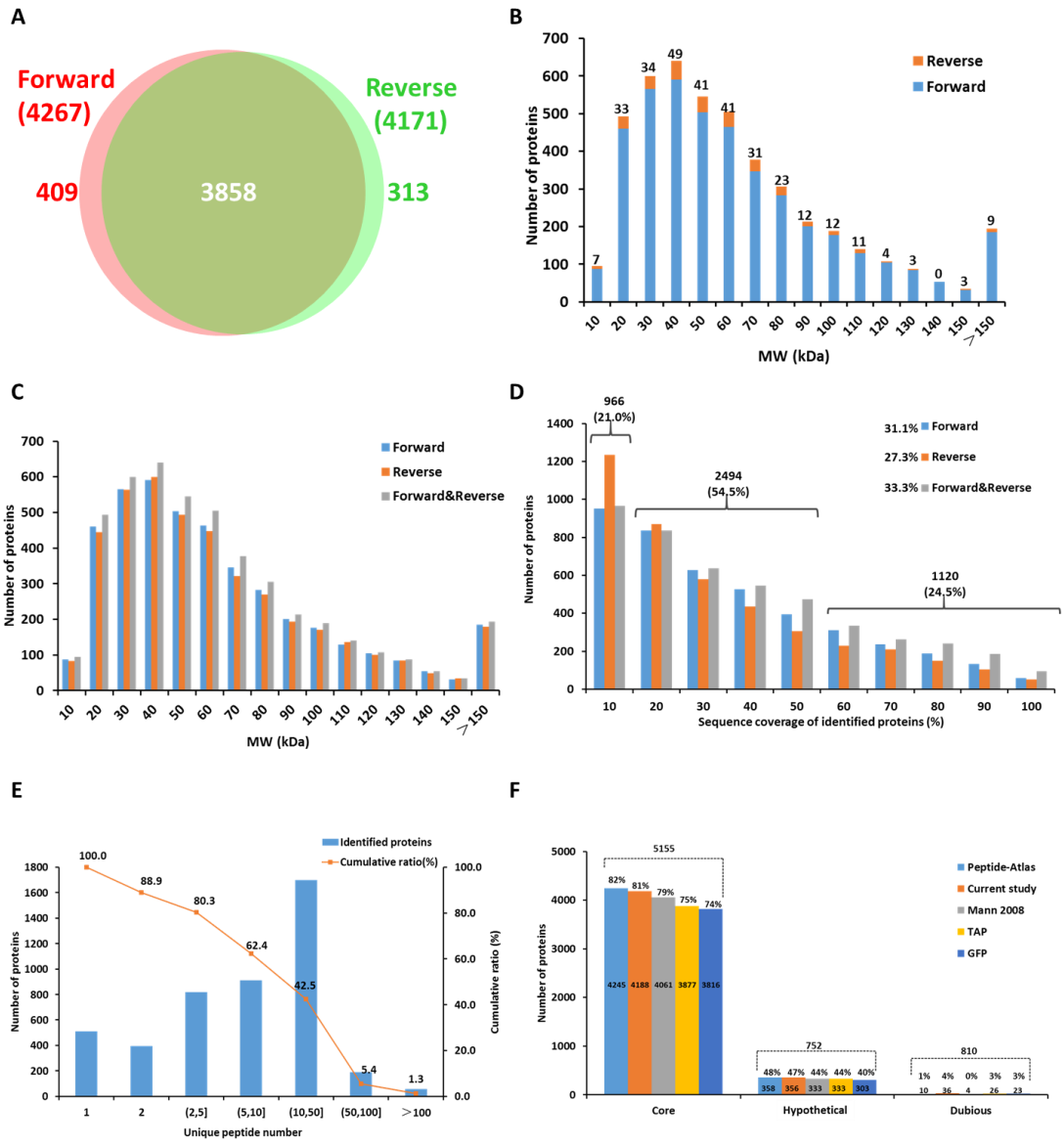

Figure S1. Proteome coverage achieved using the reported SILAC label-swap approach, Related to Figure 1.

(A) Venn diagram of proteins identified in forward and reverse experiments.

(B) MW distribution of proteins identified in forward and reverse experiments. The number above the column represents the number of unique proteins added by the reverse experiment.

(C) MW distribution of proteins identified in forward and reverse experiments.

(D) Sequence coverage of identified proteins by different experimental strategies. Percentage on the right of the legend represents the average sequence coverage of corresponding proteins. The number above the bracket represents the sum of the corresponding proteins. The percentage in the bracket represents the proportion of the corresponding proteins among all the proteins identified in the proteome. The

average sequence coverage of our dataset is as high as 33.3%, which insures the depth and accuracy of our proteomic study.

(E) Number of unique peptides in identified proteins. The number on the left *y*-axis represents the sum of proteins among each bin of peptide number. The percentage on the right *y*-axis represents the cumulative ratio of proteins with peptides greater than or equal to each bin.

(F) Comparison of proteome coverage of MS-based proteomic strategies from this study with four datasets of Mann 2008, Peptide Atlas, GFP- and TAP-tagging methods among the catalogues of core, putative or hypothetical, and dubious proteins. Number above the dotted line represents the sum of each catalogue. Percentage above the bar represents the coverage of each dataset for the corresponding catalogue.

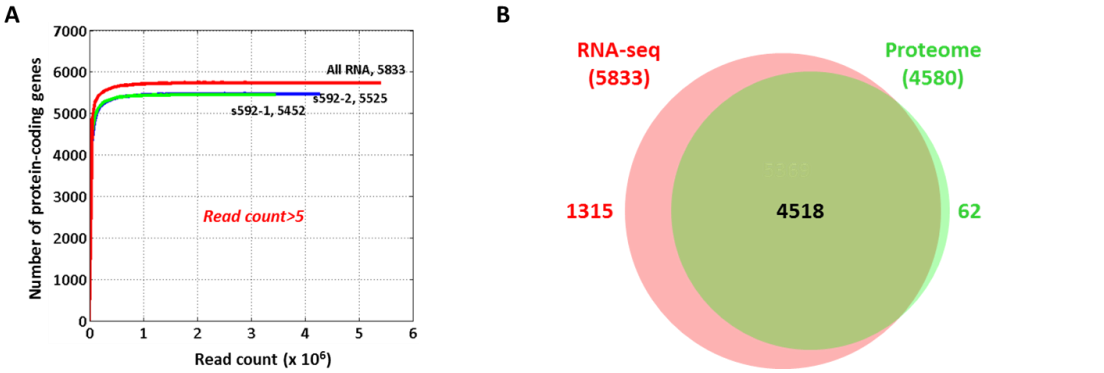

D

Pseudogenes identified by current proteome dataset

Protein	Gene	MW	Mann	Peptide Atlas	TAP	GFP
YDR441C	APT2	20	1	1	1	1
YPR081C	GRS2	71	1	1	1	1
YAR073W	IMD1	44	1	0	0	0
YIL170W	HXT12	51	1	0	0	0

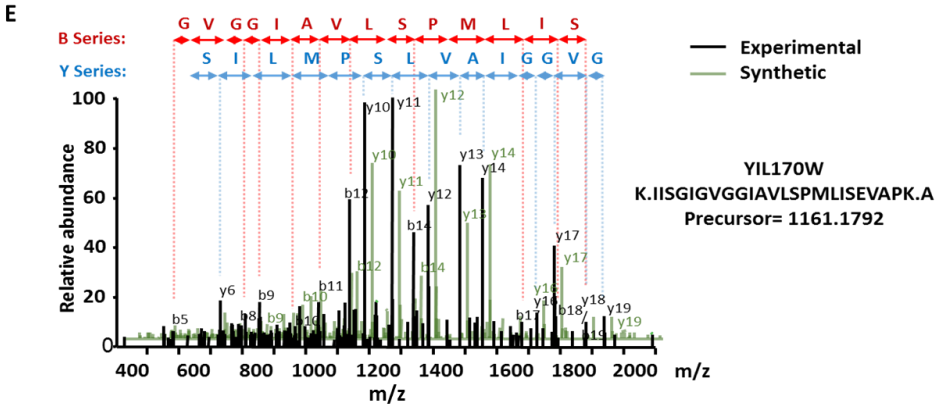

Figure S2. Characteristics of in-depth RNA-seq analysis, Related to Figure 1 and Figure 2.

(A) Saturated coverage of yeast transcriptome by deep RNA-seq analysis. An estimate of the number of actively expressed protein-coding genes based on the number of uniquely mapped RNA-seq reads is shown for different experiments.

(B) Comparison of the coverage of MS-based proteome and RNA-seq-based transcriptome.

(C) Identification-level coverage of RNA-seq analysis for core, put or hypo, and dubious proteins. The percentage above the bar represents the proportion of genes with identified transcripts.

(D) Overview of the pseudogenes identified by our proteome dataset. One of these pseudogenes, YIL170W, was selected for validation.

(E) Comparison and validation of the MS2 spectra of the identified peptide generated from the pseudogene YIL170W in large scale proteomics with that of the synthetic peptide.

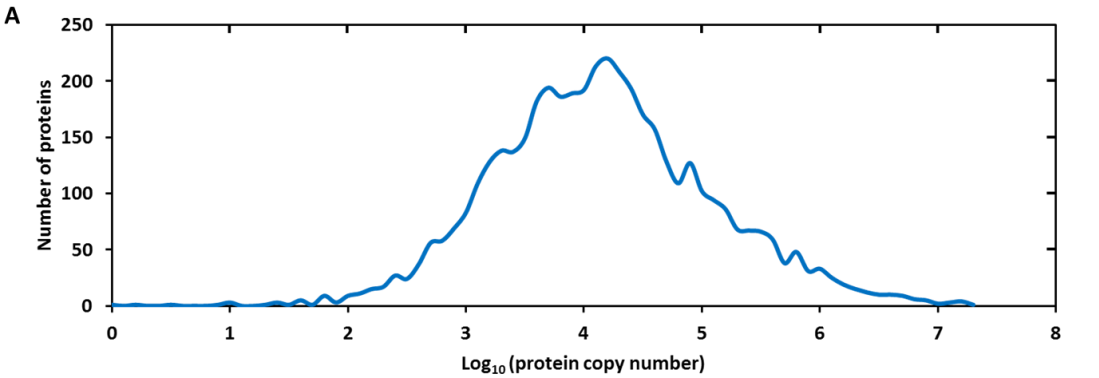

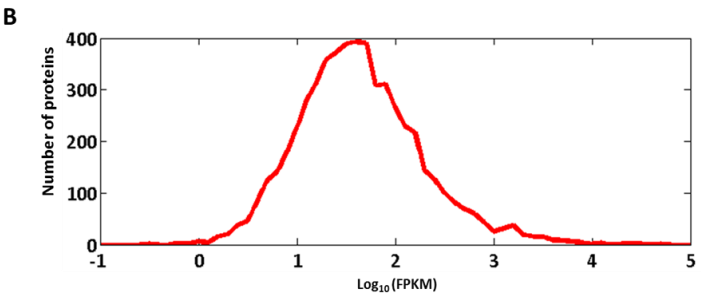

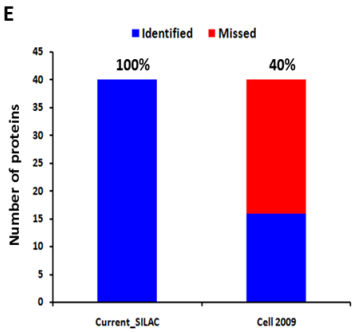

C

In-depth coverage of the dataset

Coverage or Percentage	Proportion (%)
Proteins with GO annotations	72.3
Cell membrane proteins	76.6
Transcription factors	80.0
Pathways with >75% coverage	86.0
Pathways with 90% coverage	38.0
Average coverage for all pathways	84.2

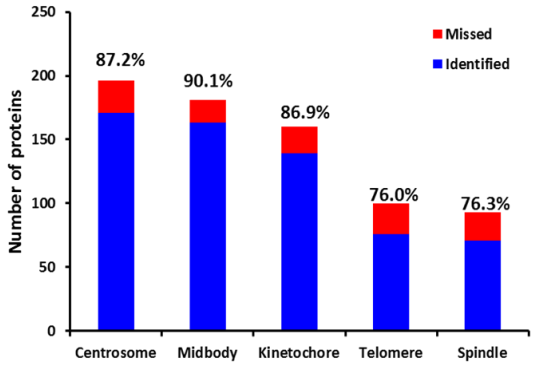

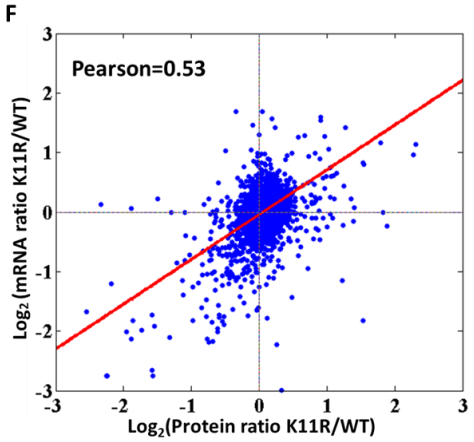

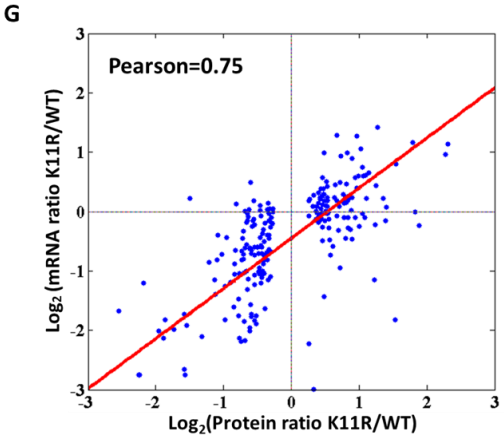

Figure S3. High coverage in our SILAC quantification experiment, Related to Figure 1 and Figure2.

(A) Dynamic range of protein abundance.

(B) Dynamic range of mRNA abundances.

(C) Protein coverage of the different biological pathways.

(D) High coverage for five sub-proteome functioning in mitosis.

(E) Coverage of the methionine biosynthesis pathway for current study and our previous study of Xu et al., 2009.

(F) Correlations for all quantified proteins. The *x*-axis and *y*-axis represent changes in the proteome and transcriptome, respectively.

(G) Correlations for proteins with significant changes in the proteome. The *x*-axis and *y*-axis represent changes in the proteome and transcriptome, respectively.

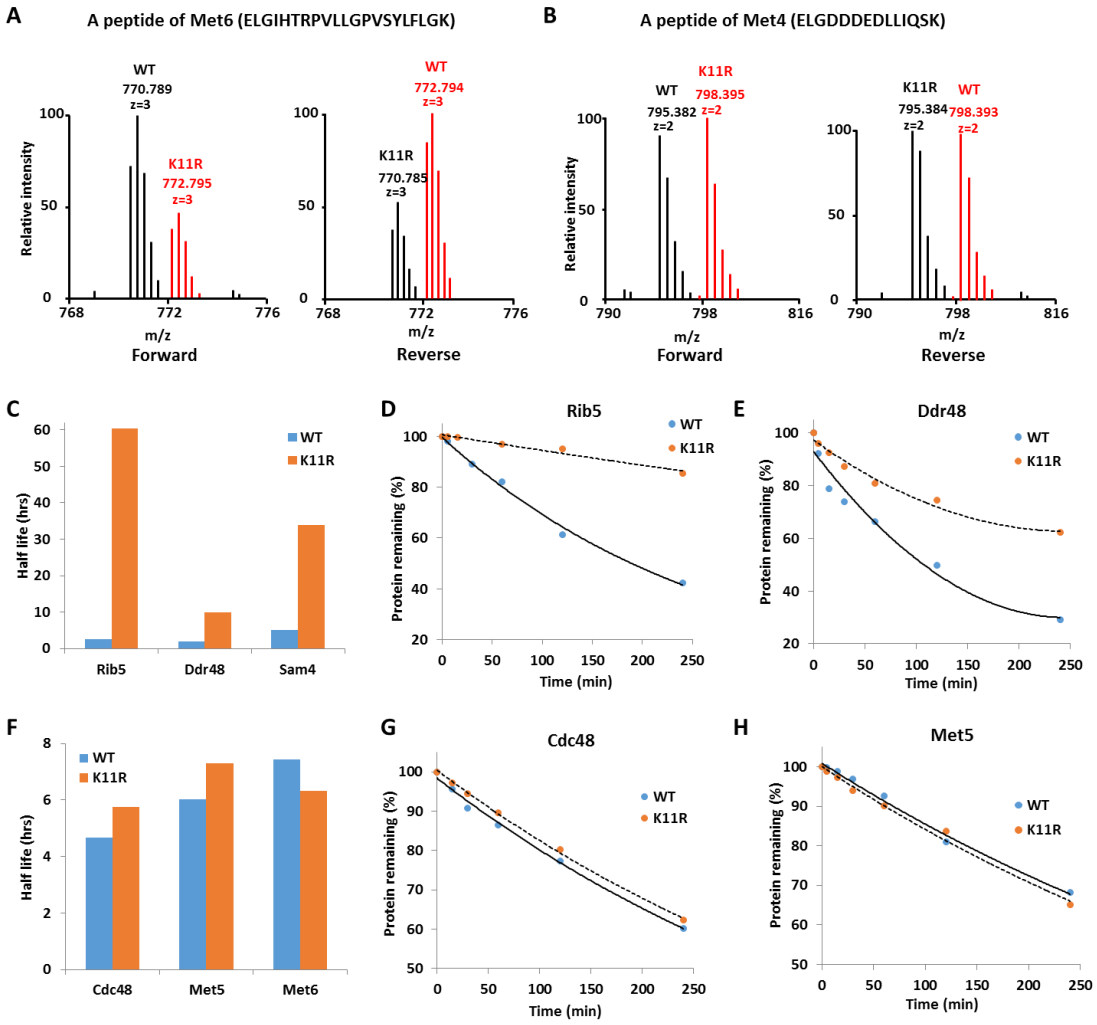

Figure S4. Half-life analysis of the changed proteins in the K11R strain and related genes within methionine synthesis pathway, Related to Figure 2 and Figure 3.

(A) Isotope-labeled peptide pairs of Met6 from forward (left) or reverse (right) experiments. Light- and heavy-labeled peptides were distinguished by their m/z

ratios.

(B) Isotope-labeled peptide pairs of Met4 from forward (left) or reverse (right) experiments. Light- and heavy-labeled peptides were distinguished by their m/z ratios.

(C) Half-life time comparison of the changed proteins in K11R strain, including Sam4, Rib5 and Ddr48.

(D and E) Decay curves were presented for the Rib5 and Ddr48, respectively.

(F) The half-life time comparison of the unaffected proteins, including Cdc48, Met5 and Met6.

(G and H) Decay curves were presented for the Cdc48 and Met5, respectively. The x-axis and y-axis represent pulse chase time and protein remaining after shifting yeast cells from heavy to light medium. These proteins were as the negative control, which were not affected in K11R mutant strain.

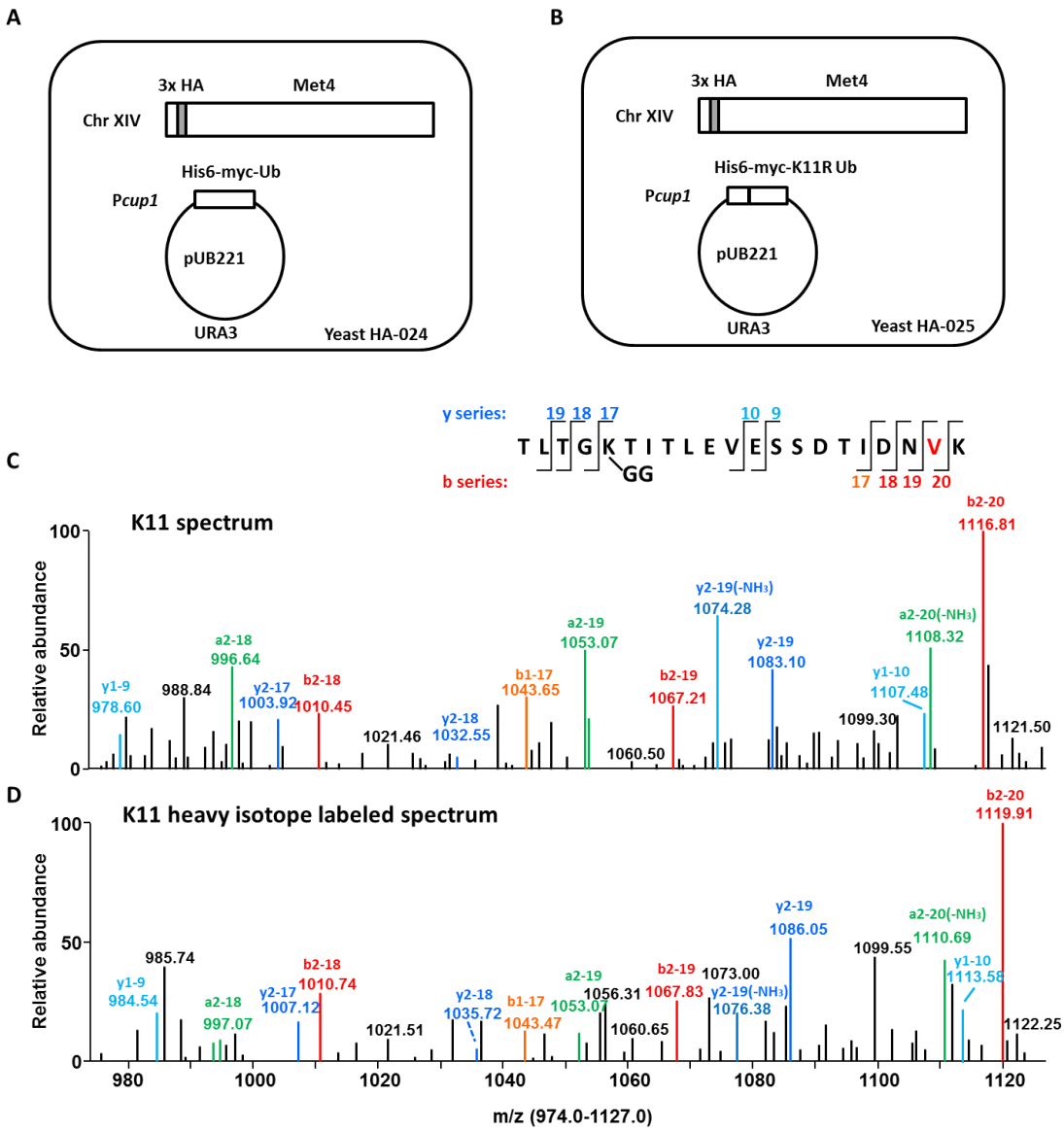

Figure S5. Identification of K11 linkages on 3HA-tagged Met4 proteins, Related to Figure 4.

(A and B) Schematic of WT (A) and K11R (B) expressing 3HA-tagged Met4.

(C and D) Mass spectrum of the K11-linked peptides identified on 3HA-tagged Met4 proteins after trypsin digestion. The sample is mixed with synthetic heavy-labeled GG remnant modified lysine peptides and measured with SRM for abundance of ubiquitin linkage-specific peptide, representing the abundance of this modification. The mass spectrum of synthetic heavy-labeled K11-linked peptides is shown at the bottom (D). The mass spectrum of detected K11-linked peptides on 3HA-tagged Met4 proteins is shown at the top (C). The two mass spectra are almost identical except for the mass shift caused by heavy isotopes.

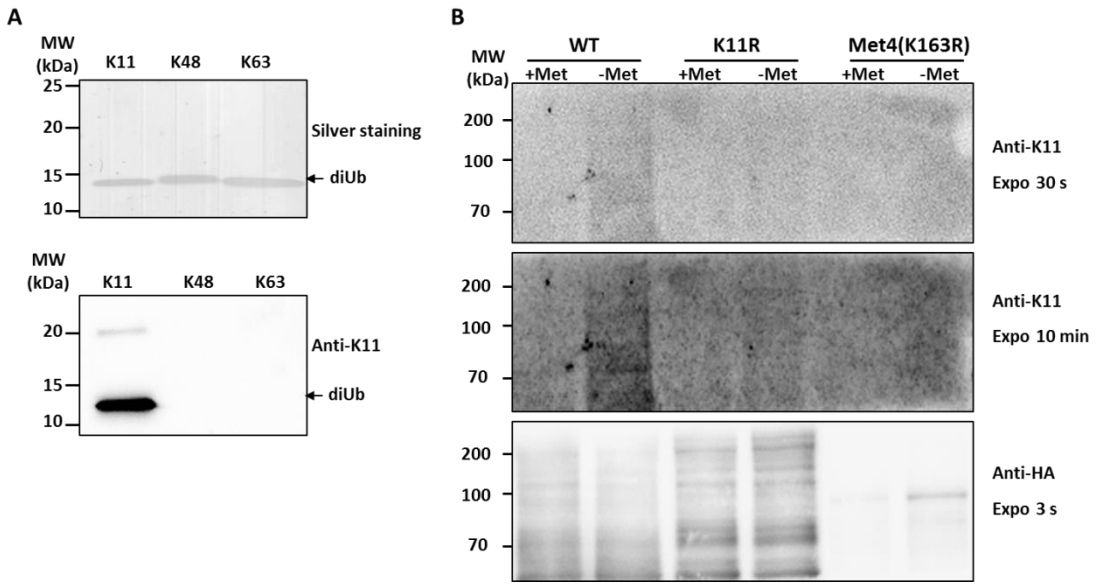

Figure S6. Increase of K11-linked ubiquitin chains on Met4 after methionine depletion, Related to Figure 4.

(A) Equal amounts of K11-, K48-, and K63-linked di-ubiquitin were loaded and detected through silver staining (up panel). The K11 specific antibody was used to confirm specificity for K11-linked chain (lower panel).

(B) The K11 selective antibody was used to probe HA-Met4 immunoprecipitates from WT as well as K11R mutant yeast strains, and cells expressing MET4-K163R. HA-Met4 was immunopurified from these strains grown under normal and methionine depleted growth conditions.

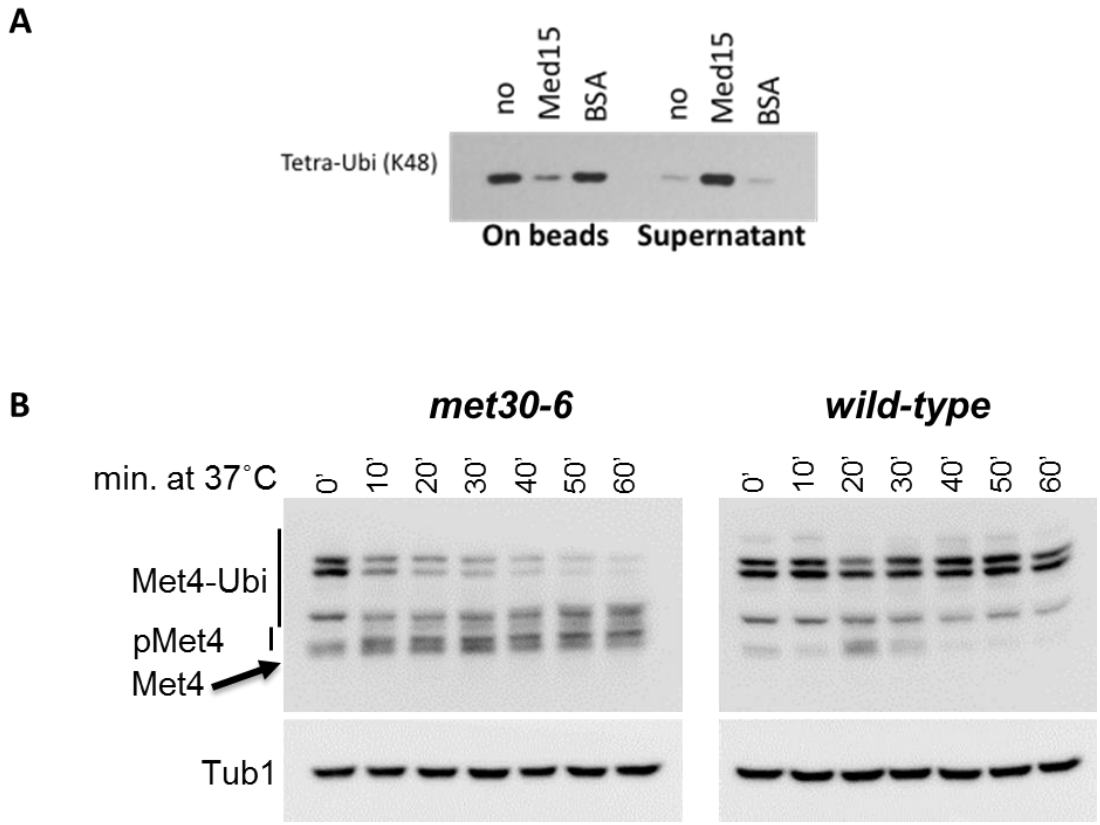

Figure S7. Med15 competes with K48 ubiquitin chains to bind on UBD domain of Met4, this process was deubiquitination-dependent, Related to Figure 6.

(A) Med15 but not BSA competes with ubiquitin binding on Met4. Immobilized Met4 (76-160) was bound to K48 tetraubiquitin. Elution of K48 tetraubiquitin by addition of 3-fold molar excess of Med15 (residues Med15 1-651 Δ239-271, Δ373-483) or BSA was analyzed by immunoblotting of the eluted fraction and the bead bound fraction using anti-ubiquitin antibodies.

(B) Wild type cells and temperature sensitive *met30-6* mutants were grown at 28˚C to an OD_{600}= 0.6, shifted to 37˚C to inactivate the temperature sensitive $SCF^{Met30-6}$ ligase, and samples were collected at the time intervals indicated. Total cell extracts were separated by SDS-PAGE (7.5%) and Met4 was detected with anti-Met4 antibodies. Tubulin was detected as a loading control. The decrease in ubiquitylated Met4 reflects deubiquitylation kinetics because the half-life of Met4 is >60min.